JOM, Vol. 74, No. 2, 2022
https://doi.org/10.1007/s11837-021-05058-2

Application of Transition Metal Phosphides to Electrocatalysis: An Overview

NAVID ATTARZADEH ,[1,2,5] RAVINDRA NUGGEHALLI,[3] and C.V. RAMANA[1,4]

1.—Center for Advanced Materials Research, University of Texas at El Paso, 500 W. Univ. Ave, El Paso, TX 79968, USA. 2.—Environmental Science and Engineering, University of Texas at El Paso, 500 W. Univ. Ave, El Paso, TX 79968, USA. 3.—Department of Physics, New Jersey Institute of Technology, University Heights, Newark, NJ 07102, USA. 4.—Department of Mechanical Engineering, University of Texas at El Paso, 500 W. Univ. Ave, El Paso, TX 79968, USA. 5.—e-mail: nattarzadeh@utep.edu

Recently, sustainable energy alternatives have attracted the scientific community and policymakers as concerns over global warming and depletion of fossil fuels have increased significantly. Substituting H_2 gas as a primary source for our daily energy consumption under the guideline of the hydrogen economy concept has not progressed as anticipated because of inadequate efficiency associated with the generation (electrolyzer) and utilization (fuel cell) devices. A critical challenge is to design strategies for fabricating electrocatalysts derived from earth-rich elements to address cost and performance concerns. In this context, nanostructured transition metal phosphides (TMPs) have emerged as highly efficient electrocatalysts. The excellent electrocatalytic performance of TMPs is ascribed to their suitable charge transfer from metal to phosphorous as well as the easy transfer process of a proton-coupled electron during hydrogen evolution reaction. This overview focuses on the materials fabrication and the associated challenges in the design and development of TMP-based catalysts.

INTRODUCTION

Preserving the environment by establishing global-scale sustainable energy systems has emerged as one of the most vital and critical challenges for the future generation.[1,2] The projection of energy demands required for the growing world population and industrialization expansion illustrates 24–26 TW under scenarios of "new policies" or "current policies," while carbon dioxide emission will reach 37–44 Gt per year in 2040.[3] The energy supply demands immediate impetus to diversify energy sources, emphasizing environmental challenges aroused by fossil fuel consumption. The current momentum is to broaden the traditional power supply and to narrow the usage of fossil fuels. The daily increased demands for clean and economical energy resources provide excellent opportunities for designing and exploring new electrocatalysts which can address current global challenges related to environment and sustainability. For instance, a rational strategy is to employ electrocatalysts for converting water as an environmentally abundant source to higher-value energy sources, including hydrogen and oxygen. Nanostructured transitional metal phosphides have improved electrocatalytic activity compared to many bulk materials.[4] The efficacy of electrocatalysis is controlled by the electrode materials, which in turn determine the kinetics of hydrogen release and adsorption/desorption at the electrode-electrolyte interface. Figure 1 represents the schematic of applications of transition metal phosphides in various energy segments.

Employing electrocatalysts for either splitting water for hydrogen evolution reaction (HER) and oxygen evolution reaction (OER) or operating cathodic processes of oxygen reduction reaction (ORR) show a remarkable potential to maximize

(Received August 18, 2021; accepted November 17, 2021; published online January 14, 2022)

Fig. 1. Schematic representation of modulated strategies for modification of transition metal phosphides for energy-related applications.

energy density economically and efficiently in fuel cells. In this respect, the essential goal is to develop precious metal-free catalysts demonstrating well-controlled nanostructures that augment the number of active sites and high durability and sufficient intrinsic activity at each site. The application of nanostructured electrodes made from transition metals (Ni, Co, Mo, etc.) has been studied extensively as electrocatalysts because of their abundant earth reserves and active properties. In recent decades, electrocatalysts composed of earth-rich transition metals that are utilized for energy transformation could be categorized as follows: transition metal oxides (TMO),[5] metal nitrides (TMN),[6,7] metal dichalcogenides (TMDs),[8–10] metal carbides (TMC),[11] and insulated single atoms of transition metals (TMs).[12] For example, the well-known electrocatalysts developed for specific reactions are MoS_2 for HER[13,14] and Co_3O_4 for OER/ORR.[15,16] Despite the current progress of the noble metal-free paradigms, a few challenges such as inadequate active sites and weak electron conductivity have yet to be addressed to achieve the primary milestones in the development of electrocatalysts. TMPs have demonstrated significant physicochemical characteristics such as desirable electronic features because metal-rich metal phosphides are metallic, even acting as superconductors.[17] Crystalline surfaces in TMPs provide more active sites, in contrast to 2D TMDs, where catalytic activity relies on the edges of stacking layers.[18] Broader stability in various pH conditions endows greater applicability to TMP structures. Due to excellent physicochemical features and several fabrication methods, TMP electrocatalysts surpass constraints seen in TMO, TMN, and TMDs and represent greater feasibility to replace noble metal catalysts. All elements known as transition metals in the periodic table can react with phosphorous to form TMPs. Phosphides demonstrate complex chemistry because different crystalline structures emerge from different stoichiometric ratios, and minor variations in the ratio of metal to phosphorous result in a significant alteration in physicochemical characteristics.[19] Thus, it seems rational to record better electron conductivity and chemical stability when metal-rich or monophosphide TMP structures are provided because of adequate metal–metal bonds and metal-phosphorous bonds compared to phosphorus-rich TMPs with good phosphorous-phosphorous bands.[17] Therefore, the favorable physicochemical features of TMPs can be tuned successfully by altering their

corresponding compositions and structures.[20] For instance, a key frontier in the synthesis of new structures is to tailor the composition and structure of electrocatalysts to operate at various conditions while researchers pursue improving the longevity and selectivity of catalysts to realize the prospects of replacing renewable energy with fossil fuels.

The reversible reaction of hydrogen evolution, reaction (1), occurs on the electrode surface and requires being catalyzed by an electronic conductor:[21]

$$H^{+}_{(aq)} + e^{-} \rightarrow {}^{1}/_{2}H_{2(g)} \quad (1)$$

Indeed, the chemical composition and surface structure of the electrode strongly influence the rate of hydrogen evolution, known as electrocatalytic activity. Generally, the hydrogen evolution (HER) can be categorized into three steps in the acidic environment:[21]

1. Volmer or discharge reaction:

$$H^{+}_{(aq)} + e^{-} \rightarrow H_{ad} \quad (2)$$

2. Tafel or combination reaction:

$$2H_{ad} \rightarrow H_{2,ad} \quad (3)$$

3. Heyrowsky or ion + atom reaction

$$H^{+}_{(aq)} + H_{ad} \rightarrow H_{2,\,ad} \quad (4)$$

After the reaction between electrons from electrode and protons from solution, the surface of the catalyst requires adsorption of H_{ad} and formation of molecular hydrogen gas. The electrocatalytic activity can be defined using the Butler-Volmer equation,[21] relating the reaction current density j to overpotential η, and the exchange current density,j_0, and is proportional to the reaction rate, as shown by Eq. 5:

$$j = j_0\left[\exp\left(\frac{\alpha F\eta}{RT}\right) - \exp\left(\frac{-(1-\alpha)F\eta}{RT}\right)\right] \quad (5)$$

Electrocatalytic activity relates to the composition, morphology, microstructure, and surface/interface features of the materials involved. This study summarizes the effective strategies to fabricate transition metal phosphides to form a significant number of exposable active sites with modified composition and structure. It focuses on regulations and effective approaches in synthesizing TMPs such as elemental doping, phase modification, structural and interfacial engineering, and incorporation of other effective supports such as nanocarbon. The future outlook and prospects are presented to offer impetus for fabricating TMP electrocatalysts with robust efficacy.

FABRICATION STRATEGIES OF TRANSITION METAL PHOSPHIDES

The methods of preparation for transition metal phosphides are presented nowadays with new strategies, which provide scale-up fabrication lines for hydrogen electrocatalyst production. Several strategies have been developed to control the size, composition, and morphology of prepared nanostructured TMPs. The fundamentals of fabrication methods are categorized into processes that are tightly associated with phosphorous sources. For instance, the preparation of active HER catalysts such as Ni_2P nanoparticles, FeP nanosheets, and CoP nanoparticles has suffered from including several tedious steps involving organic solvents.[22–25] Subsequently, studies shifted towards developing organic solvent-free strategies such as phosphorizing Co_3O_4 at 300°C for 2 h to prepare highly active HER catalysts of hybrid CoP nanocrystals supported by carbon nanotubes (CoP/CNT).[26] Sun's group has conducted pioneering studies on a series of nanostructured metal hydroxides (including Co, Ni, Fe, and Cu) and synthesized nanostructured assays of TMPs without the involvement of organic phosphorous sources.[26–32] In this study, we focus on fabrication strategies that rely on inorganic phosphorous sources. The flammable and noxious natures of organic phosphorous sources have hampered the development of methods using them. However, implementing inorganic and elemental phosphorous sources has resulted in the progress of multiple eco-friendly fabrication strategies. Sun et al. fabricated CoP on carbon cloth (CC) using phosphorization in a porcelain boat at 300°C for 60 min in a static Ar atmosphere.[27] They also electrodeposited nanosheet arrays of α-$Co(OH)_2$ on a Ti plate at room temperature followed by phosphorization in a porcelain boat with $Na_2H_2PO_2$ at 300°C for 1 h.[33] The merit of growing nanostructure arrays on the current collectors such as carbon cloth (CC) is to prevent using a polymer binder, while TMP arrays remain well retained and coupled tightly with the electrode.[27]

Solution-Phase Reaction Methods

This fabrication method usually proceeds in highly boiling point solvents, including 1-octadecene and oleylamine at an elevated reaction temperature of approximately 300°C to cleave strong C–P bonds in organophosphorus such as trioctylphosphine (TOP) or triphenylphosphine (TPP) and their analogs as phosphorous sources.[34] For instance, metal acetylacetonates as the metal precursor participate in a reaction with TOP,[35] given by the following chemical formula:

$$(C_8H_{17})_3P + M(\text{acetylacetonate})_2 \rightarrow MP_x \quad (6)$$

After cleaving C–P bonds at high temperatures, the phosphorous atoms can coordinate with metal atoms to create metal phosphides. This reaction route can end up producing well-defined crystalline and nanostructured 3*d*, 4*d*, and 5*d* transition metal phosphides.[17]

One of the early studies to prepare TMPs through the solution-phase method reported the formation of single crystalline Ni_2P nanowires, in which the ratio of TOP to oleic acid controlled the formation of one-dimensional nanowires.[36] For instance, the preparation of Ni_2P nanoparticles supported on SiO_2 through a reaction between Ni(acetylacetonate)$_2$ and trioctylphosphine resulted in the formation of a uniform particle size distribution and the efficient evolution of H species relating to a facile transfer of H species from nickel sites to the support.[37] Henkes et al. also reported a solution-mediated reaction involving TOP and preformed transition metal nanoparticles as precursors.[38] They produced a broad range of transition metal phosphides, including Ni_2P, Rh_2P, Au_2P_3, PtP_2, and PdP_2, and could tune size, size disparity, and hollow sphere formation by controlling parameters of the metal nanoparticle precursors. Stern et al. prepared highly uniformly distributed Ni_2P nanowires by heating Ni(acetylacetonate)$_2$ in a solution containing oleic acid, trioctylamine, and tri-n-octylphosphine.[39] They compared the catalytic activity of Ni_2P in the two structures of nanowires and nanoparticles, which was synthesized through a simple thermal reaction of NaH_2PO_2 and $NiCl_2{\cdot}6H_2O$. They found that the nanoparticles exhibited lower overpotentials at the same loading quantity on the carbon substrate. Therefore, the characteristics of TMPs can be controlled by tailoring organic solvents, the molar ratio of metal to phosphorous, and the reaction temperature. This method requires rigorous control of the reaction condition and continuous purge of inert gas to prevent leakage of flammable gases.[36]

However, electrodeposition is an eco-friendly method that will not release highly toxic substances into the environment. In this approach, a thin film of Ni is fabricated using the electrodeposition method from ethylene glycol/choline chloride (EG/ChCl) and then is phosphorized into Ni-P using organic phosphorous solution.[40] A crystalline/amorphous Co/CoP film is also prepared on Ni foam using one-step electrodeposition at ambient conditions.[41] The obtained Co-P film shows catalytic activity and strong bonding with the substrate resembling low interface resistance and intensified H evolution. The constraints of this method are its limited applications to specific Ni-P and Co-P compositions and the lack of uniformity of the deposited metal phosphides, while their structures are also amorphous.[37] Recently, the electrodeposition process has been utilized to fabricate nanocomposite of NiP_x/TNAs. The NiP_x/TNAs composites show superior electrocatalysts activity toward HER due to enhanced electrocatalytic active sites from amorphous NiP_x. Figure 2 illustrates the performance and preparation steps for NiP_x/TNA nanocomposite electrocatalysts. TEM and HRTEM images of the sample are shown in Fig. 2. The lattice spacing of 0.35 nm relates to the anatase titanium oxide phase with (101) plane, while a low quantity of NiP_x crystal phase is detected. The detailed elemental distribution of NiP_x/TNAs nanocomposites is shown by EDS analyses of participating elements.[42]

Gas-Phase Reaction Methods

Transition metal phosphides can be obtained after reaction between highly active phosphorous steam source and either metal vapor or nanostructured metal precursors at temperatures ranging from 300 to 900°C, and the chemical formula can be expressed as MP_x.[38] The adverse outcome can be the possibility of producing P-rich metal phosphides (i.e., CoP_3) and even some unstable metal phosphides.[17] Besides, a cautious approach needs to be taken at elevated temperatures to prevent the escape of noxious phosphorous source gases such as phosphine, and the seal of the reaction furnace needs rigorous control. At temperatures > 250°C, PH_3 is released and reacts with the metal oxides to produce metal phosphides.[36] Employing this strategy is beneficial because the nanostructure morphology of metal oxides is most likely retained after reaction at a temperature of 300°C for approximately 2 h.

Plasma-assisted synthesis of TMPs also shows promising results for catalytically producing oxygen and hydrogen. This finding has inspired researchers to perform many interesting studies benefiting from PH_3 plasma conditions to obtain NiFe-P and NiCo-P.[43] Low-temperature phosphorization of bimetallic metal-organic frameworks such as MOF-74 is an interesting method for controlling the synthesis of NiCo-P nanotubes as highly efficient electrocatalysts.[44] Optimizing the molar ratio of Co/Ni atoms in the MOF structure could result in a variety of synthesized Co_xNi_yP catalysts. The produced nanotubes show good HER and OER catalytic performance in an alkaline electrolyte, offering a low overpotential of 129 mV for H_2 and 245 mV for O_2 productions at a current density of 10 mA/cm^2. In a recent study, a multicomponent reactive low-temperature plasma-assisted simultaneous MOF decomposition and phosphorization, offering high chemical reactivity combined with low-temperature conditions, has been demonstrated.[45] Ultrafine $Ni_{12}P_5$ nanoparticles encapsulated in a thin layer of N-doped carbon (NC) show a superior HER performance under a broad pH range. The crystal structure of Ni MOF-74 is grown on Ni foam (NF) through the solvothermal reaction. Plasma conversion is performed in a horizontal quartz tube furnace. The temperature is maintained at 300°C for evaporation of red phosphorous, and NH_3 and H_2

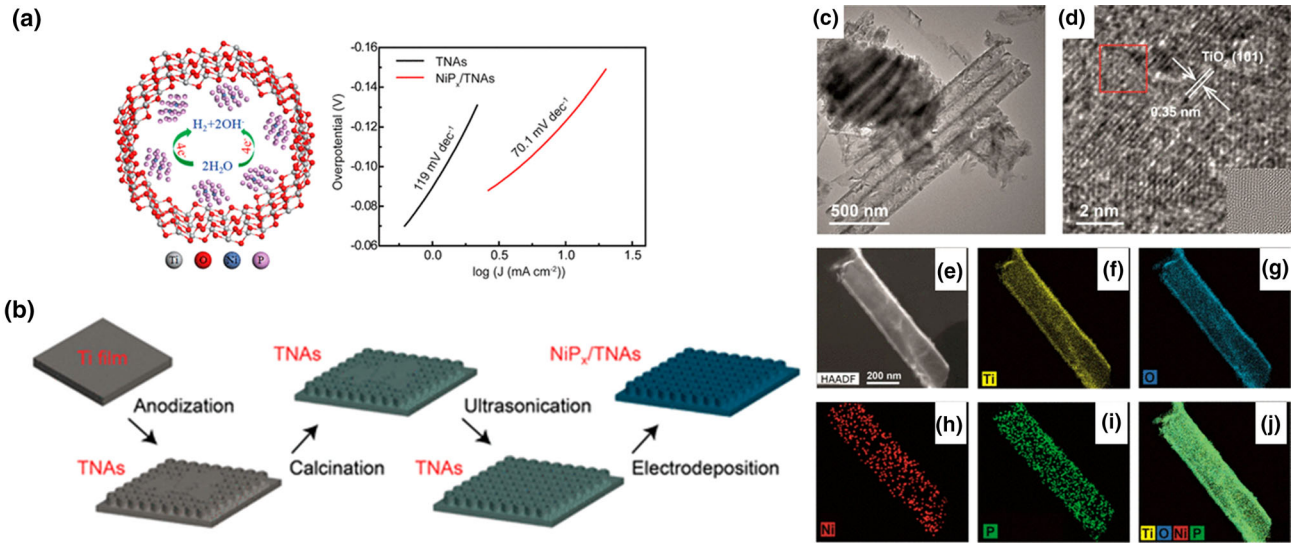

Fig. 2. (a) Illustration of the participating element in the prepared catalysts and the performance of the catalysts. (b) Schematic process of the NiP_x/TNAs preparation steps. (c, d) TEM and HRTEM images of NiP_x/TNAs nanocomposites. (e–j) EDS mapping profiles of participating elements in the NiP_x/TNAs nanocomposits.[42] Reproduced with permission from the American Chemical Society (ACS).

are introduced into the chamber. The plasma glow covers the entire hot zone where phosphorization of precursors takes place, and samples are treated with NH_3 plasma and H_2 plasma, respectively. The SEM images reveal a comparative illustration of two different structures of nickel phosphide that are well dispersed in their encapsulated situations. XRD patterns reveal two different phases of $Ni_{12}P_5$ and Ni_2P formed by NH_3 plasma and H_2 plasma, respectively, indicating that the phase structure is affected strongly by the plasma. The measurement of in situ optical emission spectroscopy (OES) reveals the presence of PH radicals in both plasma-assisted situations, in which the PH radicals are the main precursors for phosphorization at low temperatures. The ultrafine $Ni_{12}P_5$ particles, encapsulated in N-doped carbon shells, successfully show a promising performance of the hydrogen evolution reaction in a broad pH range. The plasma-assisted phosphorization method offers exciting opportunities to prepare various bimetallic phosphides.[45]

As shown in Fig. 3a, ZIF-67 nanosheets are used to synthesize Fe-CoP nanosheets using an etching-coordination strategy. ZIF-67 nanosheets are first prepared using a hydrothermal method, and then the cross channels are etched to contain guest metals simultaneously. After phosphorization at 350°C, two phases of CoP and Fe-CoP nanosheets form, as shown in Fig. 3c and d. The XRD pattern in Fig. 3e shows the presence of Fe-CoP and CoP phases.[46] The peaks for (011) and (211) crystal planes of Fe-CoP showed a positive shift, indicating the doping using Fe atoms. As shown in Fig. 3f, linear sweep voltammetry (LSV) reveals that Fe-CoP can display the best catalytic activity for the OER process. In addition, the lowest overpotential can be found for Fe-CoP nanosheets. Therefore, the defect-rich Fe-doped CoP nanosheets can be fabricated successfully through an etching procedure and show excellent stability and durability until 20 h.

Other Novel Methods

In addition to the methods discussed in the previous section, novel strategies to synthesize transition metal phosphides, which are consistent with the environment, have been developed. For instance, using the nontoxic biomass phosphorous source has attracted significant interest. As an appealing phosphating reagent, phytic acid can quickly generate the phytic acid-metal cross-linked structure because of the intense affinity between its six phosphate groups and metal cations. The benefit of this method is the possibility of implementing large-scale production of transition metal phosphides. A nontoxic and facile method for synthesizing TMPs has been introduced by using phytic acid (PA) containing six phosphonic acid groups and obtained from plant sources.[47] Pu et al. have used PA for pyrolysis of metal salts in combination with melamine as precursors to fabricate a series of TMPs encapsulated in N,P-codoped carbon (NPC) such as Ni_2P NPs@NPC, FeP NPs@NPC. They report that the encapsulation method enhances the catalytic activity in a broad range of pHs. The environmentally friendly, cost-effective fabrication strategy of using PA opens an avenue to prepare TMPs in large-scale production.

Recently, carbon derived from pinecones, in combination with ultrasound (US) and microwave (MW) techniques, has been used to anchor CoP and enhance the associated electrocatalytic activity.[48] As shown in Fig. 4, US/MW-assisted techniques have been developed for the synthesis of electrocatalysts.[49] The benefits of preparation of TMPs from

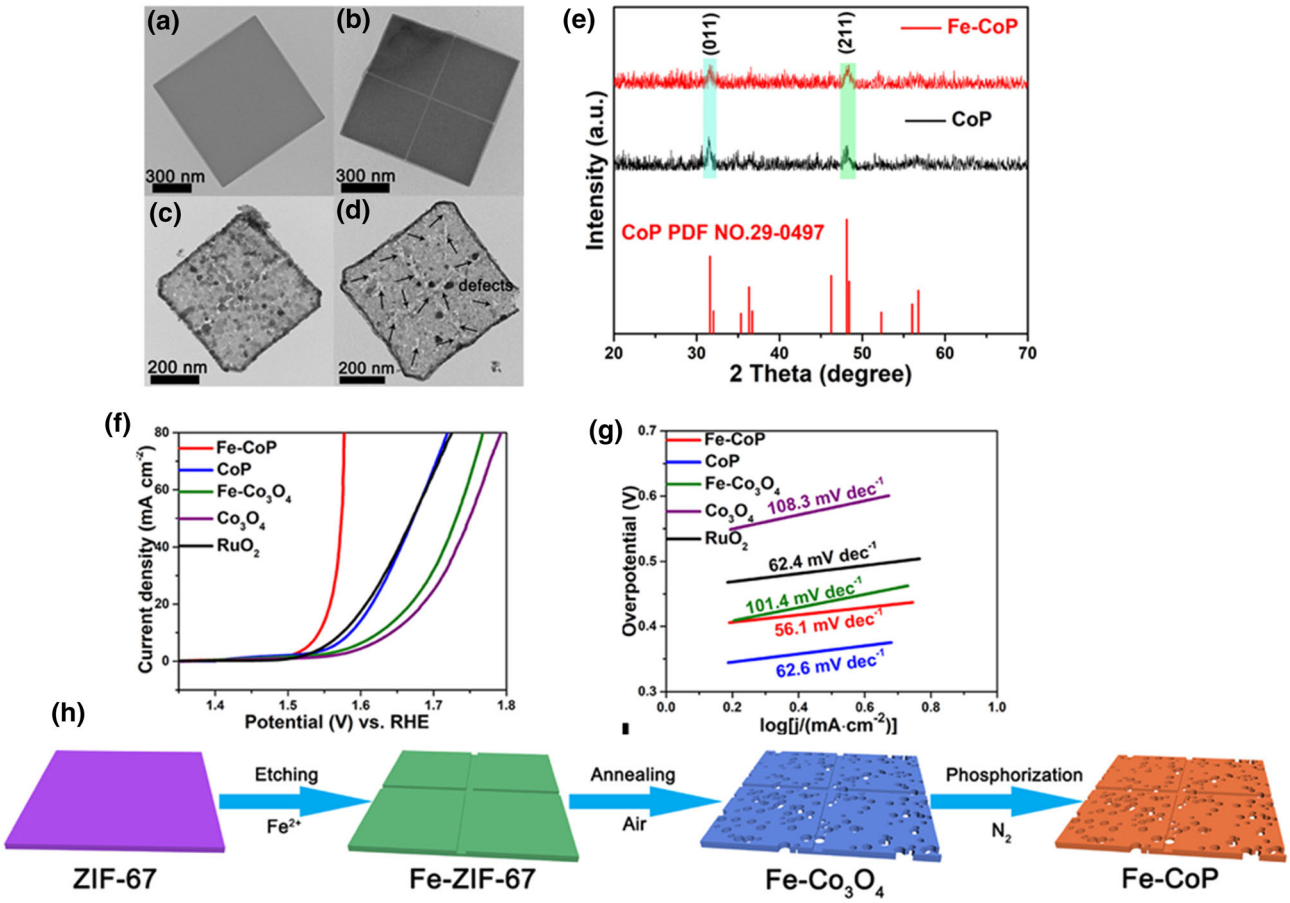

Fig. 3. (a–d) TEM images of ZIF-67, Fe–ZIF-67, Fe–Co_3O_4, and Fe–CoP nanosheets (NS), respectively. (e) Representing XRD patterns of Fe-CoP nanosheets and CoP nanosheets. (f) Linear sweep voltammetry (LSV) of Fe–CoP, CoP, Fe–Co_3O_4, Co_3O_4, and RuO_2 nanosheets. (g) Tafel slopes for the electrocatalyst performances of the same nanosheets shown in (f). (h) Schematic of the transformation of ZIF-67 to Fe–ZIF-67, Fe–Co_3O_4 after air calcination, finally phosphorization to produce Fe–CoP electrocatalysts.[46] Reproduced with permission from the American Chemical Society (ACS).

these techniques are due to the following: (1) direct transfer of energy to the proceeding reaction instead of applying heat, (i2 rate of conversion reactions being independent of applied heat, (3) feasibility of applying heat in greater rates compared to the routine process, and (4) feasibility of using material-selective heating and obtaining volumetric and local heats.[50,51] Zuliani et al. demonstrated the feasibility of preparing active CoP catalysts through biomass conversion using MW and US techniques.[48]

EARTH ABUNDANT TRANSITION METAL PHOSPHIDES

Figure 5 illustrates the most frequently used transition metal phosphides. We focus on their synthesis strategy, crystal morphology, features, and electrocatalytic performance to highlight the importance of TMPs. The successful application of nickel phosphide (Ni_2P) nanoparticles and their excellent stability in acidic solutions confirm the use of TMPs for electrocatalytic HER to produce H_2(g) with nearly faradaic yield.[20] Recent investigations also confirm that TMPs can be employed as highly efficient catalysts in OER,[39,40] thereby broadening their applications to water electrolyzers,[41] metal-air batteries,[52] and fuel cells.[42]

Covering a complete spectrum of TMPs is beyond the scope of this study. Therefore, two representative case studies, namely Ni and Co phosphides, are discussed in the following sections. It is worth mentioning that TMPs show several crystal structures, similar to different phases and structures already reported for transition metal oxides (TMOs) by our group.[53,54] The polyhedral lattice-based crystals of these phosphides are shown in Fig. 6.

A minor change in metal/phosphorous stoichiometric ratio results in a noticeable variation in structures; therefore, different physicochemical characteristics are presented. Higher electron conductivity, chemical stability, and thermal resistivity are observed in these structures. The favorable physicochemical properties of TMPs can be tested by changing composition and structure.

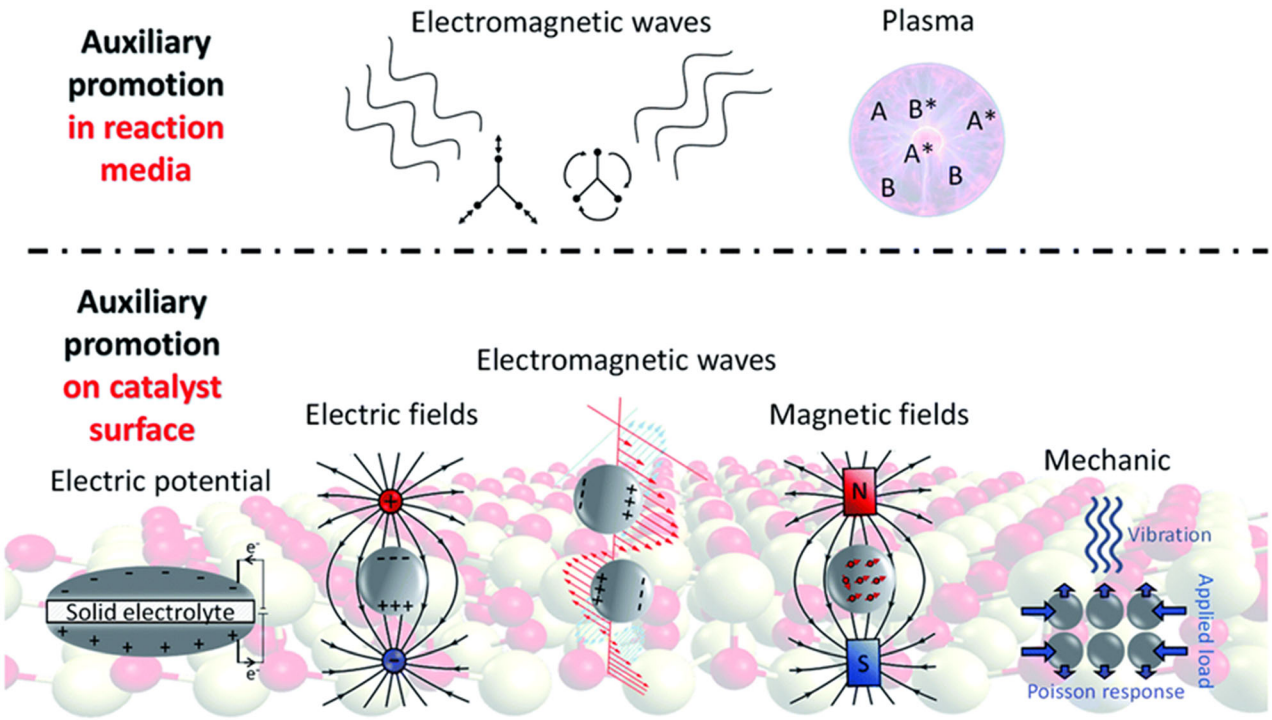

Fig. 4. An overview of techniques used for promoting reaction in the media or on the catalyst surface,[49] reprinted under a Creative Commons Attribution-NonCommercial 3.0 Unported License from Royal Society of Chemistry (RSC).

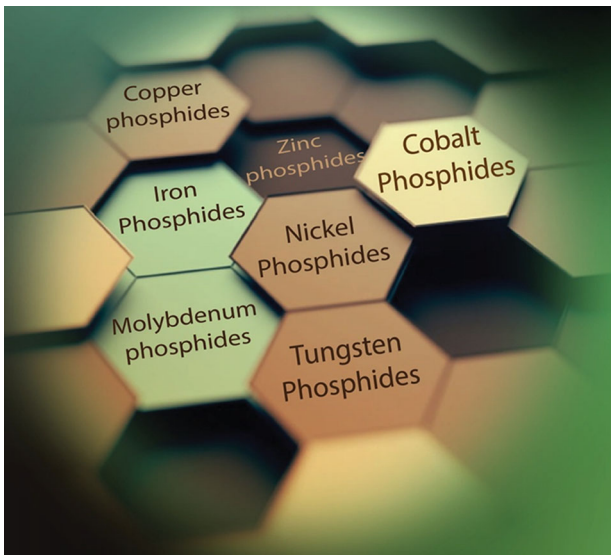

Fig. 5. Transition metal phosphides frequently used as electrocatalysts

Cobalt Phosphides

Electrocatalysts derived from CoP-based electrodes demonstrate a bifunctional catalyst. High HER activity of CoP has been observed over a broad range of morphologies, grain sizes, and preparation methods. Examples include the following: single crystals of hollow CoP nanoparticles with multiple facets on Ti foils,[22] films of CoP synthesized by cathodic deposition,[55] CoP particles on carbon cloth[28] prepared using either reaction between pre-grown Co nanoparticles and octylphosphine, or phosphidation of cobalt oxide. The aforementioned HER-active CoP studies have been conducted on polycrystalline or multifaceted nanostructures. In contrast, no information on the proportion of different crystal facets with exposable and accessible sites has been provided. It can be added that cobalt phosphides do not show magnetic properties, unlike magnetic features in cobalt ferrite compounds.[56]

To better understand the reason for the high HER activity of CoP, Popczun et al. synthesized nanostructured CoP with multiple branches that were formed by nanorod protrusions of CoP single-crystals exposing significant density of accessible (111) facets.[57] They compared the HER performance of multifaceted CoP nanoparticles with branched CoP nanorods to evaluate the role of the morphology of transition metal phosphides. Due to lack of adequate stability, the branched CoP nanostructures showed lower HER activity compared to multifaceted CoP nanoparticles. The branched CoP nanostructures showed an overpotential of 117 mV for a current density of 20 mA/cm^2, while the multifaceted nanoparticles demonstrated a lower overpotential of 100 mV for the same current density. Therefore, despite both surface areas being mutually comparable, the multi-branched CoP nanostructures showed a lower HER activity than the multifaceted CoP nanoparticles. The weak stability of the branched CoP nanostructures could be

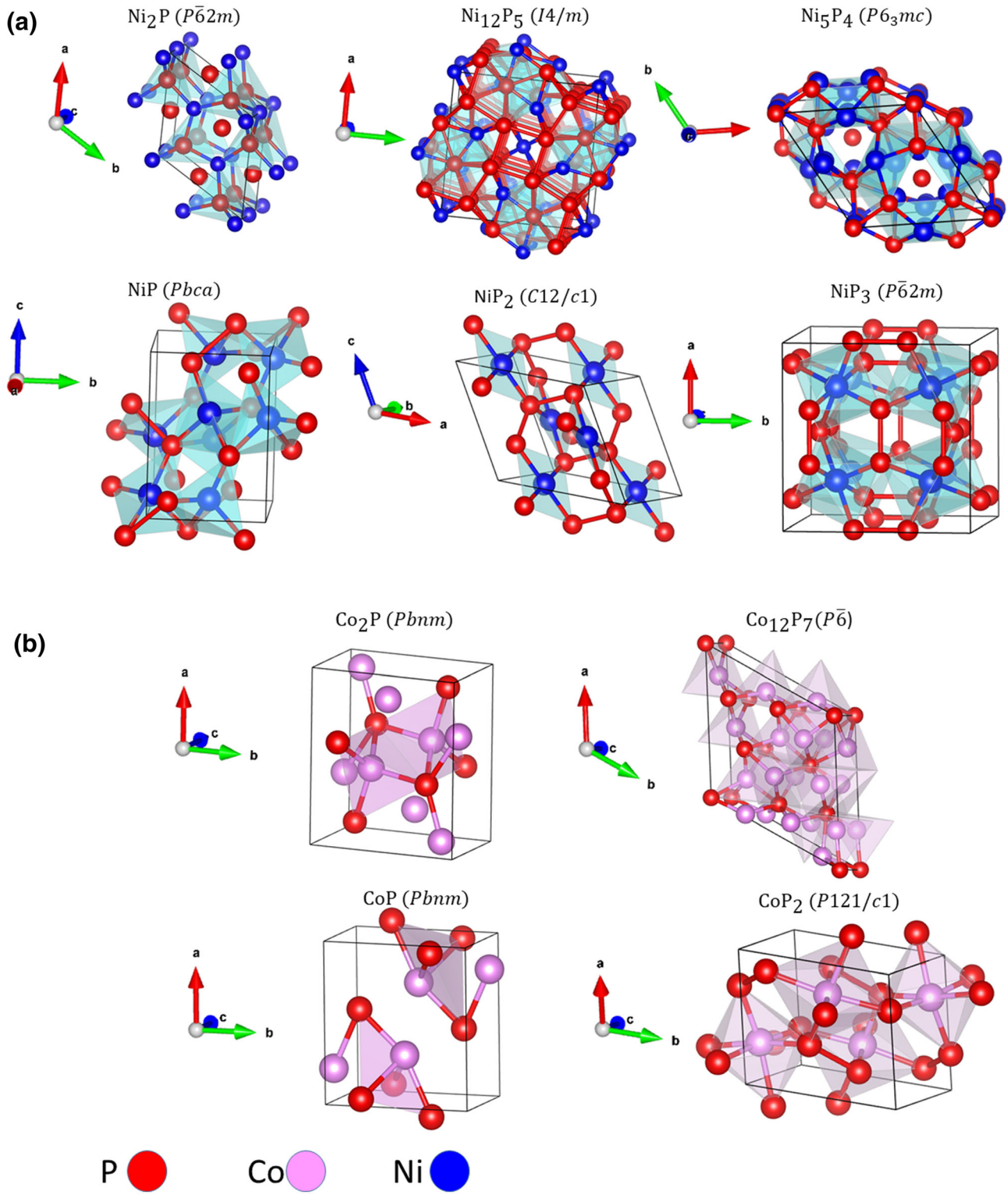

Fig. 6. Selection of the most frequently used nickel phosphides and cobalt phosphides in their polyhedral lattice-based representation.[20]

attributed to the poor adhesion of nanostructures to a Ti electrode surface.

Therefore, the importance of morphology or preparation method was removed from bottlenecks related to the high intrinsic activity of CoP-based catalysts. The general interest is to design nanoscale arrays to achieve better electrocatalytic performance and compete with the commercial Pt- and

Ru/Ir-based catalysts. Two successful examples of engineered structures are ultrathin and holey nanosheets of CoP, as they facilitate significant HER activity due to the high surface area and super hydrophilicity at the surface.[58,59] Dang et al. integrated modified ultrathin and three-dimensional (3D) holey nanostructures to produce CoP phase on the carbon cloth (CC) as a bifunctional electrocatalyst for HER at 0-14 pH values and OER in an alkaline environment.[60] Figure 7a shows the XRD characterization of the orthorhombic CoP phase and the scanning electron microscopy (SEM) images of uniformly deposited ultrathin cobalt hydroxide nanosheets (Fig. 7b, c and d), while it is apparent that the earlier morphology is probably retained after phosphidation at 300°C for vertically grown nanosheets of CoP phases (Fig. 7e, f and g). Promising electrocatalytic activity of CoP reflects the importance of the synergistic effects of 3D electrochemically grown structure facilitating the exit of gas bubbles and greatly improved effective electrolyte diffusion. Their work leads to an avenue for preparing binder-free HER electrodes in the prospect of renewable energy.

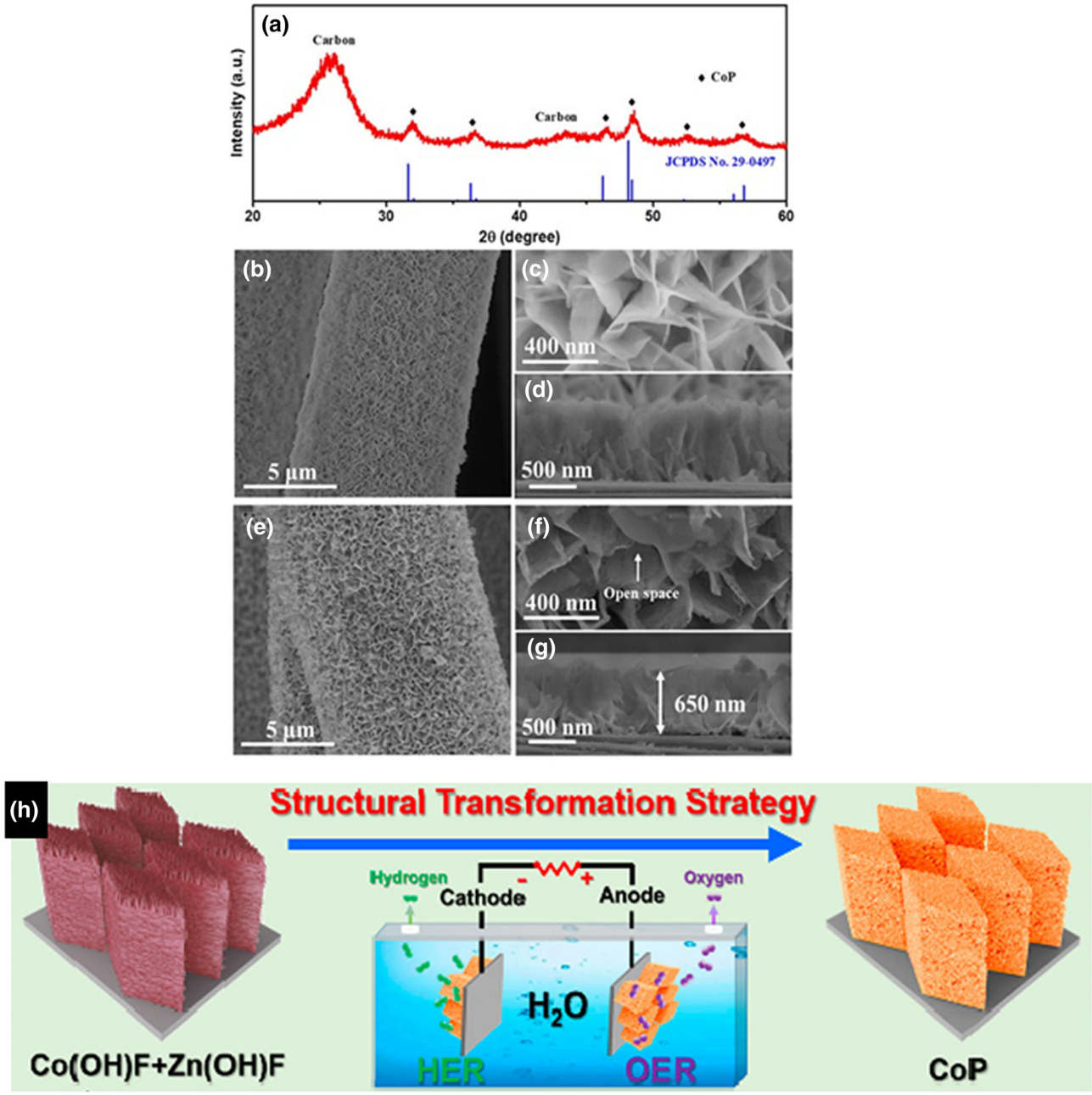

Fig. 7. (a) XRD analysis of CoP supported on CC. (b–d) SEM images of cobalt hydroxide supported on CC. (e–g) SEM images of CoP supported on CC.[60] (h) Schematic representation of the structural transformation of cobalt hydroxides to cobalt phosphides.[61] Reproduced with permission from the American Chemical Society (ACS).

To produce 3D CoP porous structures, Cao et al. conducted a controllable structural transformation strategy on the phosphatized Ni foam.[61] Removing the Zn-based compounds by alkali etching left porous Co-based compound arrays with nanoflake hierarchical structures. CoP arrays formed through the phosphorization process using $NaH_2PO_2.H_2O$ as the P source. Figure 7h shows a schematic of the structural transformation steps. The prepared CoP@NF electrode showed excellent bifunctional electrocatalytic activity for both HER and OER in alkaline electrolytes. The enhanced performance could be ascribed to the presence of large, exposed surface areas with abundant active sites. The unique morphology of CoP promoted fast gas release and electrolyte diffusion for modified kinetics of the catalyst. A recent study also reported an innovative synthesis of Fe-doped CoP nanosheets (NS) using an etching-coordination method, inspired by the merit of the two-dimensional NS, heteroatom doping, and defective structure.[46] The catalysts demonstrated many exposable active sites due to the unique topography of the two-dimensional NS structure. The doping of Fe element influenced the regulation of electron structure between Co and P.

The combination of doping with foreign elements and improving the morphology through engineered nanostructures will increase the intrinsic activity of each site and the number of active sites on a given electrocatalyst synergistically. Besides, one of the main challenges during the fabrication of cobalt phosphides is to prohibit preparation at elevated temperatures where agglomeration of phosphides hinders the mass and charge diffusion channels and diminishes the number of active sites.[62] For this purpose, Han et al. fabricated Mo-doped porous CoP nanosheets supported by nickel foam, in which synthesizing porous nanostructures was originated from removing Al from CoMo(Al)-P.[63] The prepared nanocrystalline material was composed of $Co_{0.76}Mo_{0.24}P$ with an average particle size of 4.11 nm. The modification occurred on the electrocatalyst because the impingement of Mo^{6+} and Al^{3+} led to greater dispersion of Co^{2+} in its hydroxide precursors and inhibited the formation of agglomerated CoP nanocrystals during phosphorization at elevated temperatures. Besides, the incorporation of Mo into CoP modified the electronic structure and augmented the catalytic activity by increasing the electrochemically active surface area and decreasing the resistance of the interface between catalysts and solution.[63] Jiang et al. also fabricated electrocatalysts consisting of CoMoP heterogeneous nanosheet arrays that were decorated with plenty of tiny CoP_3 nanoparticles.[64] A tremendous effort was required to form bimetal phosphides, with the aim to weaken the H bonds on P active sites. However, the modification on anion sites may cause a stronger effect on HER activity than interring the metal for cation sites because the active sites of TMPs for HER is P. For instance, N doping at the P sites of CoP_2 supported on porous carbon cloth (PCC) showed a modified HER activity.[65] It was realized that the N doping in the anion sites could ease not only the electron transit but also decrease the Gibbs free energy of hydrogen adsorption (ΔG_{H*}) on both Co and P sites, which improved HER activity. Successful incorporation of a trace amount (< 1%) of sulfur into Co_2P as a doping anion also caused modification of HER/OER catalyst activity.[66] Fabrication of N-doped Co_2P nanorod arrays, supported by carbon cloth, using a hydrothermal method confirmed enhanced electrical conductivity, increased exposure of active site number after N doping for all pH values.[67] Chen et al. also reported the fabrication of Fe-doped CoP that was inspired by the defective structure of 2D nanosheets and used an innovative approach of an etching-coordination strategy to prepare support for the catalysts.[68]

Nickel Phosphides

A significant amount of research has been performed on nickel phosphide electrocatalysts, in which composition, morphology, and microstructures were controlled to obtain superior HER catalytic activity and stability in acidic and alkaline conditions. The performance of nickel phosphides is primarily influenced by the P/Ni ratio.[25,69,70] Pan et al. reported a higher catalytic activity for the nanocrystals of Ni_5P_4 than the nanocrystals of $Ni_{12}P_5$ and Ni_2P.[69] They ascribed the superior catalytic activity of Ni_5P_4 to the higher positive charge of Ni and a more substantial ensemble effect of P in nanocrystals of Ni_5P_4.[71] The ensemble effect is recognized in which the negatively charged P reduces the affinity between M–H bonds and facilitates the quicker release of H_2 gas during desorption.[72] Nickel phosphides could form in several phases, including Ni_3P, Ni_5P_2, $Ni_{12}P_5$, Ni_2P, and Ni_5P_4.[25,65,66,69] Laursen et al. worked on the HER activity and electrochemical stability of Ni_3P, whose phosphorous content is the lowest among the thermodynamically stable nickel phosphide phases.[73] Their work confirmed that the pure crystalline phase of Ni_3P microparticles could show excellent HER activity (slightly lower than that of Ni_5P_4) with high corrosion resistance in both acidic and alkali solutions despite its low phosphorous content. Figure 8a shows the chronopotentiometry (CP) analysis of Ni_3P, Ni_5P_4 microparticle catalysts comparatively in acidic and alkali solutions during 16 h. The cyclic voltammetry (CV) analysis of Ni_3P, Ni_5P_4, and Pt in acidic and alkali conditions is shown in Fig. 8b. It is apparent that the Ni_3P phase could show a catalyst activity close to that of Ni_5P_4. Figure 8c depicts the plot of current density vs. overpotential for Ni_3P phase in acidic and alkali conditions. Figure 8d illustrates a comparison between electrocatalyst performance metrics for Ni_3P and other state-of-the-art HER electrocatalysts in the acidic condition.

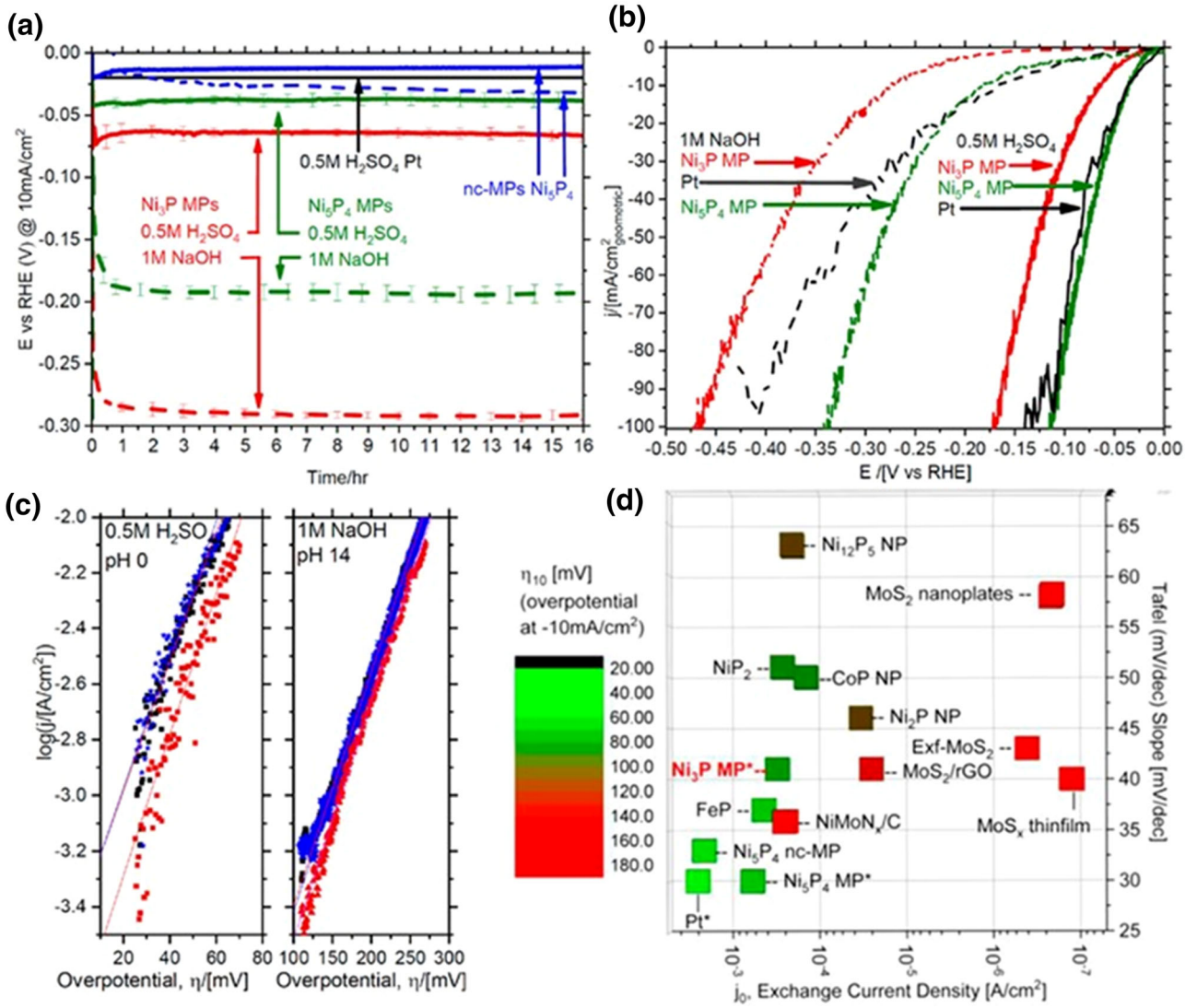

Fig. 8. (a) Chronopotentiometry of different electrodes in acidic and alkali condition. (b) Cyclic voltammetry of different electrode compositions in acidic and alkali condition at a scan rate of 1 mV/s. (c) Tafel plots of Ni_3P at acidic and alkali conditions. (d) Comparison of three electrocatalyst performances for different electrode materials.[73] Reproduced with permission from the American Chemical Society (ACS).

These results confirm the high intrinsic activity of Ni_3P microparticles and the excellent corrosion tolerance under reduction conditions for both acidic and alkali. Due to added effect of ionic Ni–P bonding, this extra bonding for the case of Ni_3P causes a larger heat of formation and greater corrosion resistance. The boosted stability of Ni_3P compared to Ni(s) can be quantified by the heat of formation of Ni_3P ($\Delta H_f = -220$ kJ/mol) versus Ni(s) ($\Delta H_f = 0$ kJ/mol). As P content rises for Ni_3P, Ni_5P_2, and Ni_2P, the per-atom stability stays relatively constant. The authors deduced that the change in the bonding configurations of the Ni_3-hollow could be attributed to the structural difference between the Ni-rich structure of Ni_3P and the P-rich structure of Ni_2P and Ni_5P_4, which influences ΔG_H of phases and the HER activity of catalysts.[73]

The general understanding is that the HER activity of nickel phosphides increases with the P/Ni ratio, while the work by Laursen et al. showed an exception. The relation between HER activity and the P extent has been described by the ensemble effect [53] or ligand effect[74] between Ni and P. Similar to HER activity, tolerance against degradation can also be related to the P/Ni ratio, where the increasing ratio implies the formation of insoluble nickel phosphides in acidic condition.[69] An innovative study of one-step TMP fabrication presents electrodeposition of highly stable nickel phosphide phases followed by a selective leaching process.[75] In this study, the additional deposited metallic Ni is dissolved at positive potentials; the nickel phosphides are stable. The porous structures remaining after leaching metallic nickel result in more extensive surface contact for the intensified HER activity.

The application of bimetallic phosphides on the self-supported porous NiCuC foil shows efficient HER performance.[76] The porous Ni–Cu alloy template is prepared in association with graphite carbon using the powder metallurgy method, where the direct phosphorization at 300°C produces a hierarchical porous structure of Ni_2P–Cu_3P@NICuC catalyst. The prepared catalyst consists of laterally grown Ni_2P aggregates with plenty of vertically attached small particles of Cu_3P, providing significant surface contacts and remarkable interaction in the system synergistically. The bimetallic phosphides are obtained with substantial control over the phase composition because of the porous structure of the Ni–Cu template and controlling of the Ni/Cu ratio using various quantities of both precursors.[76] Recently, a super-hydrophilic hierarchical bimetallic phosphide of Ni_2P–CuP_2 has been prepared on Ni-foam and graphene carbon nanotube (CNT) heterostructure using metallic electrodeposition followed by phosphorization.[77] The porous chrysanthemum flower-like heterostructure provides a significant super-hydrophilic surface area for HER activity. Figure 9a shows the schematic representation of fabrication steps of bimetallic phosphide Ni_2P–CuP_2 on top of Ni–Gr–CNTs. It illustrates the deposition steps of Ni and Cu during the preparation of electrocatalysts. XRD patterns also confirm the formation of both phosphide phases on the CNT matrix. The detailed analyses of phases and structural configuration of the prepared catalysts are conducted by x-ray diffraction (XRD), shown in Fig. 10b.

Heterogeneous 3D graphene on top of the 3D configuration of Ni foam boosts the feasibility of increased surface area for catalytic activity, as illustrated in Fig. 10a and b. Using CNTs with the random distribution provides a highly porous network, in which intertwined and interconnected branches facilitate passivation of the electrolyte ion diffusion, generating tunnels with high conductivity for electron transfer and facilitating modified electrode support. After electrodeposition of Ni uniformly on the CNT matrix, the anchored Ni_2P phases on the CNT bundles are generated using phosphorization, thereby forming a 3D porous Ni–Gr–CNTs–Ni_2P heterostructure (as shown in Fig. 10d). To further enhance the HER activity, CuP_2 is also added to the system through electroplating of Cu followed by phosphorization, as shown in Fig. 10e. The zoomed-in view shown in Fig. 10f illustrates the morphology of the bimetallic phosphide of Ni–Gr–CNTs–Ni_2P–CuP_2 resembling a chrysanthemum flower-like bundle structure where bundle size varies from 1 μm to 3 μm. The stability of the catalysts is confirmed by a chronoamperometry test at a cell voltage of 1.45 V, where Fig. 10m illustrates that the catalysts can be maintained at least for 40 h with a negligible deviation of 3% from the current density. This result confirms the excellent and robust electrocatalytic performance for overall water splitting.

The traditional fabrication techniques are strenuous and render a random distribution of nickel phosphides all over the electrode, thereby weakening the connection between the catalysts and the current collector. Therefore, switching to the novel, facile, and eco-friendly strategies for HER fabrication is desirable because they provide a high-surface-area current collector and immobilized earth-rich HER catalysts. The crucial concern is to optimize the interfacial contacts between nickel phosphides and electrode substrate to augment catalytic activity. For that purpose, the direct

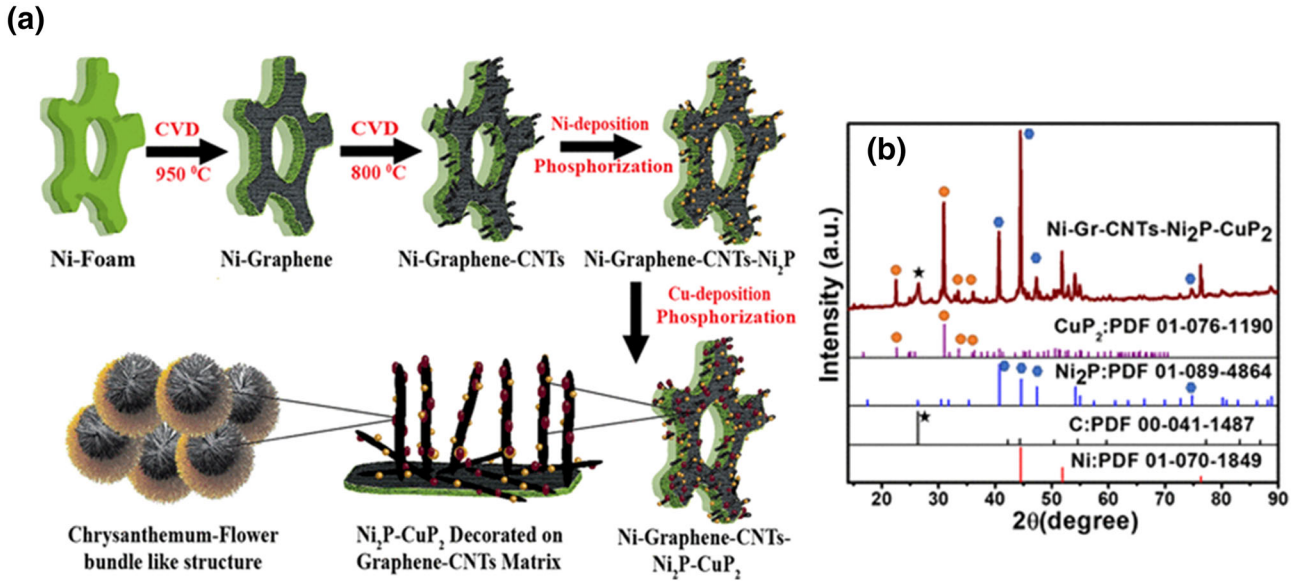

Fig. 9. (a) Schematic illustration of the preparation path of the chrysanthemum flower-like bundles of hierarchical bimetallic phosphide catalysts. (b) XRD pattern of Ni–Gr–CNTs–Ni_2P–CuP_2.[77] Reproduced with permission from the American Chemical Society (ACS).

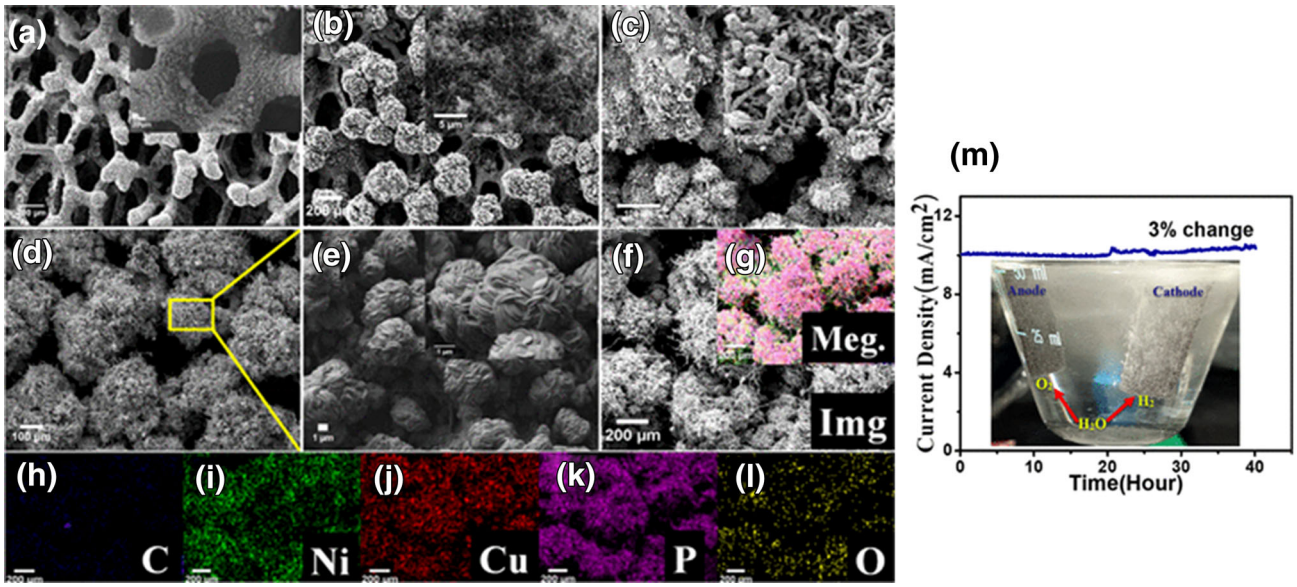

Fig. 10. (a) SEM images of graphene deposited on nickel foam uniformly in which all areas are covered homogeneously. (b) A dense CNT bundle on the graphene, where the inset confirms the random orientation and intertwining to each other. (c) Ni–Gr–CNTs–Ni_2P heterostructure (NGCN), where Ni_2P rods are anchored over CNT bundles. (d) Presence of Ni_2P and CuP_2 heterostructure on the Ni–Gr–CNTs matrix. (e) High-resolution image of Ni–Gr–CNTs-Ni_2P-CuP_2 heterostructure, with the chrysanthemum flower-like structure. (h–l) EDS elemental mapping images for the heterostructure shown in (f) for C, Ni, Cu, P, and O elements, while (g) represents the merged image of all the elements. (m) The chronoamperometric study of stability at an applied voltage of 1.45 V in alkaline solution.[77] Reproduced with permission from the American Chemical Society (ACS).

growth of nickel phosphides on the substrate, known as binder-free methods, has gained significant attention among researchers.[74,78] Recently, one-step synthesis of NiP_x electrocatalysts without subsequent phosphorization at elevated temperature has been reported by Gao et al. on TiO_2 nanotube arrays.[75] First, the vertically aligned TiO_2 nanotube arrays are prepared by anodic dissolution. Then, well-ordered nanotubes are used for co-deposition of nickel and phosphorous to provide a high-contact surface area and boost catalytic activity. This geometry provides an efficient charge transfer and significant capability for mass transport of hydrogen gas during electrocatalysis.[75]

SUMMARY AND OUTLOOK

Comprehensive studies performed on using transition metal phosphides for electrocatalyst applications have been summarized. The relationship between the structure and high electrocatalytic performance of TMPs is also discussed. Although rapid progress has been made for TMPs to develop versatile catalysts, detailed information of reaction mechanisms and clear classification of strategies to facilitate catalytic activity is generally inadequate. Despite the increasing number of research efforts, there are numerous opportunities and challenges in the fabrication of TMPs with enhanced performance. While a deeper understanding of the influence of processing parameters on the growth and phase warrants continued efforts, there can be more interesting ways to improve the catalytic performance of TMPs by doping. Therefore, the effect of other TM metal dopings on the structure and electrocatalytic performance will be interesting for designing efficient catalysts. Although there are some efforts already described in the literature, a more detailed account of such doping-induced effects is necessary, and further investigation is warranted. Future studies can lead to a safe, simple, sustainable, and large-scale fabrication of TMPs. The use of innovative approaches in fabrication strategies opens new avenues for TMPs.

ACKNOWLEDGEMENTS

N.A. acknowledges the technical support and encouragement provided by the Center for Advanced Materials Research (CMR), UTEP. N.A. also acknowledges the Research Associate opportunity provided by CMR, UTEP.

FUNDING

The authors acknowledge with appreciation the support from the National Science Foundation (NSF) with NSF-PREM Grant #DMR-1827745.

CONFLICT OF INTEREST

On behalf of all authors, the corresponding author states that there is no conflict of interest.

REFERENCES

1. S. Chu and A. Majumdar, *Nature* 488, 294 (2012).
2. J.A. Turner, *Science* 305, 972 (2004).

3. Z.W. She, J. Kibsgaard, C.F. Dickens, I. Chorkendorff, J.K. Nørskov, and T.F. Jaramillo, *Science* 355, 146 (2017).
4. M.P. Browne, Z. Sofer, and M. Pumera, *Energy Environ. Sci.* 12, 41 (2019).
5. F. Cheng, Y. Su, J. Liang, Z. Tao, and J. Chen, *Chem. Mater.* 22, 898 (2009).
6. M. Liu, Y. Dong, Y. Wu, H. Feng, and J. Li, *Chem. A Eur. J.* 19, 14781 (2013).
7. Y. Dong, Y. Wu, M. Liu, and J. Li, *Chemsuschem* 6, 2016 (2013).
8. N. Mahmood, C. Zhang, J. Jiang, F. Liu, and Y. Hou, *Chem. A Eur. J.* 19, 5183 (2013).
9. Y. Sun, F. Alimohammadi, D. Zhang, and G. Guo, *Nano Lett.* 17, 1963 (2017).
10. D. Kong, H. Wang, J.J. Cha, M. Pasta, K.J. Koski, J. Yao, and Y. Cui, *Nano Lett.* 13, 1341 (2013).
11. H.B. Wu, B.Y. Xia, L. Yu, X.-Y. Yu, and X.W. Lou, *Nat. Commun.* 6, 1 (2015).
12. K. Jiang, S. Siahrostami, T. Zheng, Y. Hu, S. Hwang, E. Stavitski, Y. Peng, J. Dynes, M. Gangisetty, D. Su, K. Attenkofer, and H. Wang, *Energy Environ. Sci.* 11, 893 (2018).
13. M.A. Lukowski, A.S. Daniel, F. Meng, A. Forticaux, L. Li, and S. Jin, *J. Am. Chem. Soc.* 135, 10274 (2013).
14. Y. Li, H. Wang, L. Xie, Y. Liang, G. Hong, and H. Dai, *J. Am. Chem. Soc.* 133, 7296 (2011).
15. L. Xu, Q. Jiang, Z. Xiao, X. Li, J. Huo, S. Wang, and L. Dai, *Angew. Chem. Int. Ed.* 55, 5277 (2016).
16. J. Xu, P. Gao, and T.S. Zhao, *Energy Environ. Sci.* 5, 5333 (2012).
17. J.F. Callejas, C.G. Read, C.W. Roske, N.S. Lewis, and R.E. Schaak, *Chem. Mater.* 28, 6017 (2016).
18. Y. Wang, B. Kong, D. Zhao, H. Wang, and C. Selomulya, *Nano Today* 15, 26 (2017).
19. Y. Lv and X. Wang, *Catal. Sci. Technol.* 7, 3676 (2017).
20. Y. Li, Z. Dong, and L. Jiao, *Adv. Energy Mater.* 10, 1902104 (2020).
21. L.A. Kibler, *ChemPhysChem* 7, 985 (2006).
22. E.J. Popczun, C.G. Read, C.W. Roske, N.S. Lewis, and R.E. Schaak, *Angew. Chem. Int. Ed.* 53, 5427 (2014).
23. Y. Xu, R. Wu, J. Zhang, Y. Shi, and B. Zhang, *Chem. Commun.* 49, 6656 (2013).
24. L. Feng, H. Vrubel, M. Bensimon, and X. Hu, *Phys. Chem. Chem. Phys.* 16, 5917 (2014).
25. E.J. Popczun, J.R. McKone, C.G. Read, A.J. Biacchi, A.M. Wiltrout, N.S. Lewis, and R.E. Schaak, *J. Am. Chem. Soc.* 135, 9267 (2013).
26. Q. Liu, J. Tian, W. Cui, P. Jiang, N. Cheng, A.M. Asiri, and X. Sun, *Angew. Chem. Int. Ed.* 53, 6710 (2014).
27. J. Tian, Q. Liu, A.M. Asiri, and X. Sun, *J. Am. Chem. Soc.* 136, 7587 (2014).
28. Q. Li, Z. Xing, A.M. Asiri, P. Jiang, and X. Sun, *Int. J. Hydrogen Energy* 39, 16806 (2014).
29. P. Jiang, Q. Liu, and X. Sun, *Nanoscale* 6, 13440 (2014).
30. Y. Liang, Q. Liu, A.M. Asiri, X. Sun, and Y. Luo, *ACS Catal.* 4, 4065 (2014).
31. P. Jiang, Q. Liu, Y. Liang, J. Tian, A.M. Asiri, and X. Sun, *Angew. Chem. Int. Ed.* 53, 12855 (2014).
32. J. Tian, Q. Liu, N. Cheng, A.M. Asiri, and X. Sun, *Angew. Chem. Int. Ed.* 53, 9577 (2014).
33. Z. Pu, Q. Liu, P. Jiang, A.M. Asiri, A.Y. Obaid, and X. Sun, *Chem. Mater.* 26, 4326 (2014).
34. M. Sun, H. Liu, J. Qu, and J. Li, *Adv. Energy Mater.* 6, 1600087 (2016).
35. P. Xiao, W. Chen, and X. Wang, *Adv. Energy Mater.* 5, 1500985 (2015).
36. Y. Chen, H. She, X. Luo, G.H. Yue, and D.L. Peng, *J. Cryst. Growth* 311, 1229 (2009).
37. K. Yan, Y. Li, X. Zhang, X. Yang, N. Zhang, J. Zheng, B. Chen, and K.J. Smith, *Int. J. Hydrogen Energy* 40, 16137 (2015).
38. A.E. Henkes, Y. Vasquez, and R.E. Schaak, *J. Am. Chem. Soc.* 129, 1896 (2007).
39. L.-A. Stern, L. Feng, F. Song, and X. Hu, *Energy Environ. Sci.* 8, 2347 (2015).
40. Y. Lu, C.D. Gu, X. Ge, H. Zhang, S. Huang, X.Y. Zhao, X.L. Wang, J.P. Tu, and S.X. Mao, *Electrochim. Acta* 112, 212 (2013).
41. N. Bai, Q. Li, D. Mao, D. Li, and H. Dong, *ACS Appl. Mater. Interfaces* 8, 29400 (2016).
42. S. Gao, A. Zavabeti, B. Wang, R. Ren, C. Yang, Z. Liu, and Y. Wang, *ACS Appl. Nano Mater.* 4, 4542 (2021).
43. H. Liang and H.N. Alshareef, *Small Methods* 1, 1700111 (2017).
44. L. Yan, L. Cao, P. Dai, X. Gu, D. Liu, L. Li, Y. Wang, and X. Zhao, *Adv. Func. Mater.* 27, 1703455 (2017).
45. Y. Guo, C. Zhang, Y. Wu, H. Yu, S. Zhang, A. Du, K. Ostrikov, J. Zheng, and X. Li, *J. Mater. Chem. A* 8, 10402 (2020).
46. T. Chen, S. Qin, M. Qian, H. Dai, Y. Fu, Y. Zhang, B. Ye, Q. Lin, and Q. Yang, *Energy Fuels* 35, 10890 (2021).
47. Z. Pu, I.S. Amiinu, C. Zhang, M. Wang, Z. Kou, and S. Mu, *Nanoscale* 9, 3555 (2017).
48. A. Zuliani, M. Cano, F. Calsolaro, A.R.P. Santiago, J.J. Giner-Casares, E. Rodríguez-Castellón, G. Berlier, G. Cravotto, K. Martina, and R. Luque, *Sustain. Energy Fuels* 5, 720 (2021).
49. M.J. Hülsey, C.W. Lim, and N. Yan, *Chem. Sci.* 11, 1456 (2020).
50. C.M. Cova, A. Zuliani, M.J. Muñoz-Batista, and R. Luque, *ACS Sust. Chem. Eng.* 7, 1300 (2018).
51. A. Zuliani, M.J. Muñoz-Batista, and R. Luque, *Green Chem.* 20, 3001 (2018).
52. F.H. Saadi, A.I. Carim, W.S. Drisdell, S. Gul, J.H. Baricuatro, J. Yano, M.P. Soriaga, and N.S. Lewis, *J. Am. Chem. Soc.* 139, 12927 (2017).
53. C.V. Ramana, A. Mauger, and C.M. Julien, *Progr. Crystal Growth Charact. Mater.* 67, 100533–100541 (2021).
54. C.V. Ramana, S. Utsunomiya, R.C. Ewing, C.M. Julien, and U. Becker, *J. Phys. Chem. B* 110, 10430 (2006).
55. F.H. Saadi, A.I. Carim, E. Verlage, J.C. Hemminger, N.S. Lewis, and M.P. Soriaga, *J. Phys. Chem. C* 118, 29294 (2014).
56. V.S. Puli, S. Adireddy, and C.V. Ramana, *J. Alloys Compd.* 644, 470 (2015).
57. E.J. Popczun, C.W. Roske, C.G. Read, J.C. Crompton, J.M. McEnaney, J.F. Callejas, N.S. Lewis, and R.E. Schaak, *J. Mater. Chem. A* 3, 5420 (2015).
58. J. Chang, L. Liang, C. Li, M. Wang, J. Ge, C. Liu, and W. Xing, *Green Chem.* 18, 2287 (2016).
59. Z. Fang, L. Peng, Y. Qian, X. Zhang, Y. Xie, J.J. Cha, and G. Yu, *J. Am. Chem. Soc.* 140, 5241 (2018).
60. Y. Dang, J. He, T. Wu, L. Yu, P. Kerns, L. Wen, J. Ouyang, and S.L. Suib, *ACS Appl. Mater. Interfaces.* 11, 29879 (2019).
61. S. Cao, N. You, L. Wei, C. Huang, X. Fan, K. Shi, Z. Yang, and W. Zhang, *Inorg. Chem.* 59, 8522 (2020).
62. P.C.K. Vesborg, B. Seger, and I. Chorkendorff, *J. Phys. Chem. Lett.* 6, 951 (2015).
63. Y. Han, P. Li, Z. Tian, C. Zhang, Y. Ye, X. Zhu, and C. Liang, *ACS Appl. Energy Mater.* 2, 6302 (2019).
64. D. Jiang, Y. Xu, R. Yang, D. Li, S. Meng, and M. Chen, *ACS Sustain. Chem. Eng.* 7, 9309 (2019).
65. L. Wang, H. Wu, S. Xi, S.T. Chua, F. Wang, S.J. Pennycook, Z.G. Yu, Y. Du, and J. Xue, *ACS Appl. Mater. Interfaces.* 11, 17359 (2019).
66. M.A.R. Anjum, M.D. Bhatt, M.H. Lee, and J.S. Lee, *Chem. Mater.* 30, 8861 (2018).
67. Y. Men, P. Li, J. Zhou, G. Cheng, S. Chen, and W. Luo, *ACS Catal.* 9, 3744 (2019).
68. T. Chen, S. Qin, M. Qian, H. Dai, Y. Fu, Y. Zhang, B. Ye, Q. Lin, and Q. Yang, *Energy Fuels* 35, 14 (2021).
69. Y. Pan, Y. Liu, J. Zhao, K. Yang, J. Liang, D. Liu, W. Hu, D. Liu, Y. Liu, and C. Liu, *J. Mater. Chem. A* 3, 1656 (2014).
70. A.B. Laursen, K.R. Patraju, M.J. Whitaker, M. Retuerto, T. Sarkar, N. Yao, K.V. Ramanujachary, M. Greenblatt, and G.C. Dismukes, *Energy Environ. Sci.* 8, 1027 (2015).
71. P. Liu and J.A. Rodriguez, *J. Am. Chem. Soc.* 127, 14871 (2005).

72. C. Du, M. Shang, J. Mao, and W. Song, *J. Mater. Chem. A* 5, 15940 (2017).
73. A.B. Laursen, R.B. Wexler, M.J. Whitaker, E.J. Izett, K.U.D. Calvinho, S. Hwang, R. Rucker, H. Wang, J. Li, E. Garfunkel, M. Greenblatt, A.M. Rappe, and G.C. Dismukes, *ACS Catal.* 8, 4408 (2018).
74. P. Liu, J.A. Rodriguez, T. Asakura, J. Gomes, and K. Nakamura, *J. Phys. Chem. B* 109, 4575 (2005).
75. J. Kim, J. Kim, H. Kim, and S.H. Ahn, *ACS Appl. Mater. Interfaces.* 11, 30774 (2019).
76. L. Yu, J. Zhang, Y. Dang, J. He, Z. Tobin, P. Kerns, Y. Dou, Y. Jiang, Y. He, and S.L. Suib, *ACS Catal.* 9, 6919 (2019).
77. S. Riyajuddin, K. Azmi, M. Pahuja, S. Kumar, T. Maruyama, C. Bera, and K. Ghosh, *ACS Nano* 15, 5586 (2021).
78. Y.H. Chung, K. Gupta, J.H. Jang, H.S. Park, I. Jang, J.H. Jang, Y.K. Lee, S.C. Lee, and S.J. Yoo, *Nano Energy* 26, 496 (2016).